

Local explicitly correlated second- and third-order Møller–Plesset perturbation theory with pair natural orbitals

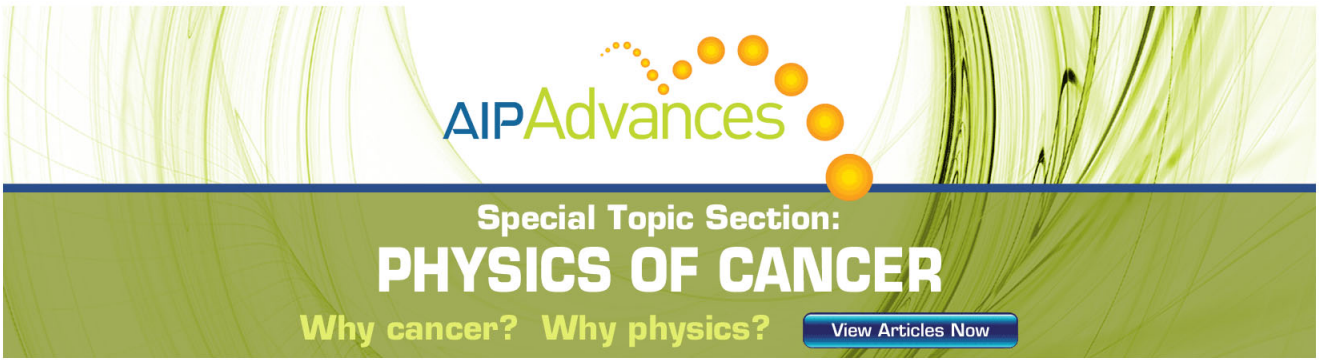
Christof Hättig, David P. Tew, and Benjamin Helmich

Citation: J. Chem. Phys. **136**, 204105 (2012); doi: 10.1063/1.4719981
View online: http://dx.doi.org/10.1063/1.4719981
View Table of Contents: http://jcp.aip.org/resource/1/JCPSA6/v136/i20
Published by the American Institute of Physics.

Additional information on J. Chem. Phys.

Journal Homepage: http://jcp.aip.org/
Journal Information: http://jcp.aip.org/about/about_the_journal
Top downloads: http://jcp.aip.org/features/most_downloaded
Information for Authors: http://jcp.aip.org/authors

ADVERTISEMENT



Downloaded 24 May 2012 to 134.147.252.238. Redistribution subject to AIP license or copyright; see http://jcp.aip.org/about/rights_and_permissions

Local explicitly correlated second- and third-order Møller–Plesset perturbation theory with pair natural orbitals

Christof Hättig,[1,a)] David P. Tew,[2,b)] and Benjamin Helmich[1,c)]
[1]*Lehrstuhl für Theoretische Chemie, Ruhr-Universität Bochum, D-44780 Bochum, Germany*
[2]*School of Chemistry, University of Bristol, Bristol BS8 1TS, United Kingdom*

(Received 5 April 2012; accepted 7 May 2012; published online 24 May 2012)

We present an algorithm for computing explicitly correlated second- and third-order Møller–Plesset energies near the basis set limit for large molecules with a cost that scales formally as $\mathcal{N}^4$ with system size $\mathcal{N}$. This is achieved through a hybrid approach where locality is exploited first through orbital specific virtuals (OSVs) and subsequently through pair natural orbitals (PNOs) and integrals are approximated using density fitting. Our method combines the low orbital transformation costs of the OSVs with the compactness of the PNO representation of the doubles amplitude vector. The $\mathcal{N}^4$ scaling does not rely upon the *a priori* definition of domains, enforced truncation of pair lists, or even screening and the energies converge smoothly to the canonical values with decreasing occupation number thresholds, used in the selection of the PNO basis. For MP2.5 intermolecular interaction energies, we find that 99% of benchmark basis set limit correlation energy contributions are recovered using an aug-cc-pVTZ basis and that on average only 50 PNOs are required to correlate the significant orbital pairs. © *2012 American Institute of Physics*. [http://dx.doi.org/10.1063/1.4719981]

I. INTRODUCTION

The pursuit of algorithms for computing electronic energies to high accuracy for sizeable molecular systems remains a central strand of research in modern chemical physics. While density functional theory is today routinely applied to systems with hundreds of atoms, progress towards reducing errors in the approximate energy functionals has been slow. Many wave function methods, canonical coupled-cluster approaches in particular, are reliably accurate, but suffer from a steep scaling of computer resources with system size, which limits their application to relatively small systems.[1] The steep scaling, however, is an artefact of the canonical representation of the wave function and Hamiltonian matrix elements and can be greatly reduced by adopting alternative representations that permit exploitation of the short-range nature of the inter-electron repulsion.

Typically, the orbitals of the Hartree–Fock (HF) reference wave function are localised through orbital rotations,[2–4] so that correlation between electrons in spatially distant orbitals becomes vanishingly small and can be neglected. Furthermore, a local basis for the virtual orbitals is selected in which the correlating cluster functions are represented using only the virtuals spatially close to the occupied orbitals. With these ingredients, it is possible to compute correlation energies with a cost that scales linearly with system size.[5,6]

Several methods involving different choices for the virtual orbitals and different algorithms for determining the cluster functions have been proposed. Schütz and Werner have championed an *ansatz* originally developed by Saebø and Pulay,[6,7] which uses non-orthogonal projected atomic orbitals (PAOs) as virtuals, combined with *a priori* selection of atom domains for each local orbital.[8–10] Since the domains are predetermined, the correlation treatment is highly efficient, but these methods have only a limited error control since the accuracy is limited by the appropriateness of the domain choices. The PAO approach has been combined[11–14] with F12 explicitly correlated methodologies,[15–19] which greatly reduce the computational cost for a given accuracy by removing the necessity for large AO basis sets with functions of high l quantum number. Other approaches which exploit the locality of dynamic correlation include the natural linearly scaling methods of Flock *et al.*,[20,21] the divide-expand-consolidate approach of Jørgensen and co-workers,[22,23] the incremental approaches of Stoll[24,25] and Friedrich and Dolg,[26–28] and the cluster-in-molecule method of Li *et al.*,[29] which all involve partitioning the molecule into a set of smaller coupled local systems. These approaches parallelise readily, but involve a high level of redundancy.

Recently, Neese and co-workers[30–32] have revived Meyer's pair natural orbital (PNO) approach,[33] where the basis of non-orthogonal virtuals are selected adaptively based on model amplitudes. The PNO representation is near optimally compact for pair theories, but has the drawback that integrals must be transformed to different virtual orbitals for every occupied orbital pair. Nevertheless we believe that the potential for efficient low-scaling PNO-based correlation treatments is high. In Ref. 34 we presented a PNO-MP2-F12 method that returns 99% of basis set limit correlation energy using only 20 virtuals on average to correlate each significant orbital pair. Two of us have also shown that a PNO-based approach for excited states is accurate and balanced and that the truncation error with respect to the canonical result can be controlled through a single parameter.[35]

[a)]Author to whom correspondence should be addressed. Electronic mail: christof.haettig@rub.de.
[b)]Electronic mail: david.tew@bristol.ac.uk.
[c)]Electronic mail: benjamin.helmich@rub.de.

 © 2012 American Institute of Physics

Downloaded 24 May 2012 to 134.147.252.238. Redistribution subject to AIP license or copyright; see http://jcp.aip.org/about/rights_and_permissions

Yang *et al.*[36] have forwarded tensor factorisation as a powerful unifying framework within which to examine alternative representations of the wave function and Hamiltonian matrix elements. In pair theories, such as second- and third-order Møller–Plesset perturbation theory (MP2 and MP3), one of the key objects is the matrix of doubles amplitudes t_{ab}^{ij} for the first-order wave function

$$|\Psi^{(1)}\rangle = \hat{T}_2|\mathrm{HF}\rangle, \tag{1}$$

$$\hat{T}_2 = \sum_{i>j,a>b} t_{ab}^{ij} a_{ij}^{ab}. \tag{2}$$

We use the convention that $i, j, \ldots$ are localised spin-orbitals occupied in the (unrestricted) Hartree–Fock determinant $|\mathrm{HF}\rangle$, $a, b, \ldots$ are canonical virtual spin-orbitals, and a_{ij}^{ab} is the second quantisation double excitation operator. Yang *et al.* observed that Pulay and Saebø's PAO (Ref. 7) and Meyer's PNO (Ref. 33) representations are two choices for tensor factorisation of the doubles amplitudes. This led them to a third factorisation, orbital specific virtuals (OSVs), which is intermediate between the PAO and PNO representations,

$$t_{ab}^{ij} = \sum_{\mu\nu} t_{\mu\nu}^{ij} L_a^{\mu} L_b^{\nu} \qquad \text{PAO}, \tag{3}$$

$$t_{ab}^{ij} = \sum_{\mu_i\nu_j} t_{\mu_i\nu_j}^{ij} L_a^{\mu_i} L_b^{\nu_j} \qquad \text{OSV}, \tag{4}$$

$$t_{ab}^{ij} = \sum_{\mu_{ij}\nu_{ij}} t_{\mu_{ij}\nu_{ij}}^{ij} L_a^{\mu_{ij}} L_b^{\nu_{ij}} \qquad \text{PNO}. \tag{5}$$

The matrices L_a^{μ}, $L_a^{\mu_i}$, and $L_a^{\mu_{ij}}$ are the transformation coefficients between the molecular orbitals a and the PAOs μ, OSVs μ_i, and PNOs μ_{ij}, respectively. The auxiliary orbitals for PAOs, OSVs, and PNOs are defined such that they are localised near an atom, a localised occupied orbital, or a pair of localised occupied orbitals, respectively. Since electron correlation is short-range, the number of non-negligible auxiliary indices is in a localised description independent of system size and each of the three tensor factorisations is compact.

We note, however, that the above factorisation for PAOs is only representative in the limit of no truncation of the PAO space. In practice, localisation is enforced by setting $t_{\mu\nu}^{ij}$ to zero unless μ and ν belong to a predefined domain of PAOs for the pair ij. With this restriction the PAO factorisation actually becomes that of Eq. (5), where μ_{ij} are now the subset of PAOs μ used for pair ij.

Yang *et al.* considered two choices for OSV representation. The first is the direct factorisation of Eq. (4), which is readily extended to triple and higher excitations. The second uses Eq. (5) but where the $L_a^{\mu_{ij}}$ are non-redundant sets of orbitals formed from the union of $L_a^{\mu_i}$ and $L_a^{\mu_j}$. Yang *et al.* found this second choice more robust to truncation of the OSV vectors in MP2 theory, and Kurashige *et al.*[37] have recently presented a procedure for optimising the OSVs.

In practice, therefore, the PNO, PAO, and (non-direct) OSV methods all utilise the same tensor factorisation. The difference between the methods lies only in the way the auxiliary orbitals are determined. For PNOs, μ_{ij} are selected that are close to optimal in that they give the most compact representation of each first-order pair function for a given target accuracy (*vide infra*). The OSV representation is much less compact, since the OSVs are optimal only for the diagonal pairs *ii*. The doubles spaces $t_{\mu_i\nu_j}^{ij}$ are therefore approximately the same size for every pair *ij*, rather than adapting to the importance of the individual pairs. The PAO representation is the least compact, since the PAOs are defined *a priori* and do not adapt to the complexity encoded in the Hamiltonian matrix elements. Conversely, the overhead in constructing and transforming to the μ_{ij} is much larger for PNOs than for OSVs than for PAOs. In PAO methods, integrals must be transformed only once, using L_a^{μ}. For OSVs, a new set of integrals is required for each occupied orbital, since they depend on $L_a^{\mu_i}$, whereas in PNO methods the integrals must be transformed for every pair using $L_a^{\mu_{ij}}$.

In this work, we introduce a hybrid OSV-PNO approach where the canonical virtuals are first contracted into an OSV basis, which is then subsequently contracted into a PNO basis. In this way the low orbital transformation costs of the OSV approach are paired with the compactness of the PNO doubles vectors, combining the advantages of the two approaches. Furthermore, this scheme retains the attractive feature that (with an appropriate selection of thresholds) the truncation error is controlled through a single parameter. We report a hybrid OSV-PNO method for evaluating RI-MP2 and RI-MP3 energies that scales as the fourth power of system size, without invoking domains, screening or local density fitting approximations. We detail the extension of this scheme to the explicitly correlated RI-MP2-F12 and RI-MP3(F12) methods, demonstrating the same scaling behaviour and a very early break-even point compared to a canonical calculation. We show that basis set errors in interaction energies computed at the MP2.5(F12) level of theory are, with an average of less than 40 PNOs per significant pair, already below 0.1 kcal/mol.

This paper is organised as follows: MP3(F12) theory is presented in Sec. II. Our choice of OSV and PNO definitions for the virtual and auxiliary orbital spaces are presented in Secs. III and IV, respectively. Our hybrid OSV-PNO approach is explained first for MP2 and MP3 in Sec. V and then for MP2-F12 and MP3(F12) in Sec. VI. Numerical data from test calculations, including truncation errors, timings, and scaling behaviours are presented in Sec. VII. We summarise and comment on future perspectives in the final section (Sec. VIII).

II. MP3(F12) THEORY

In explicitly correlated methods the first-order wave function is parameterised as

$$|\Psi^{(1)}\rangle = (\hat{T}_2 + \hat{T}_{2'})|\mathrm{HF}\rangle, \tag{6}$$

$$\hat{T}_2 = \sum_{i>j,a>b} t_{ab}^{ij} a_{ij}^{ab}, \tag{7}$$

$$\hat{T}_{2'} = \sum_{i>j} \sum_{x>y} \sum_{\alpha>\beta} c_{xy}^{ij} w_{\alpha\beta}^{xy} a_{ij}^{\alpha\beta}, \tag{8}$$

Downloaded 24 May 2012 to 134.147.252.238. Redistribution subject to AIP license or copyright; see http://jcp.aip.org/about/rights_and_permissions

where

$$|w_{xy}\rangle = \hat{Q}_{12}\left(\tfrac{3}{8} + \tfrac{1}{8}\hat{S}_{xy}\right) f(r_{12})|xy\rangle. \tag{9}$$

$\hat{Q}_{12}$ is the strong orthogonality projector, $f(r_{12}) = -\frac{1}{\gamma}\exp(-\gamma r_{12})$ the correlation factor[38,39] and $\hat{S}_{xy}$ permutes the spatial components of the spin-orbitals x and y in the determinant $|xy\rangle$,[40,41] which are chosen to be the active occupied orbitals. For notational convenience the geminals $|w_{xy}\rangle$ are in second quantisation expanded in a formally complete one-electron basis denoted by indices $\alpha, \beta, \ldots$ with expansion coefficients $w_{\alpha\beta}^{xy} = \langle\alpha\beta|w_{xy}\rangle$. $\hat{Q}_{12}$ is approximated with the aid of a complementary auxiliary (CA) orbital basis in two ways[42]

$$^{A}\hat{Q}_{12} = 1 - \hat{O}_1\hat{O}_2 - \hat{V}_1\hat{V}_2 - \hat{O}_1\hat{V}_2'' - \hat{V}_1''\hat{O}_2, \tag{10}$$

$$^{B}\hat{Q}_{12} = \hat{V}_1\hat{V}_2' + \hat{V}_1\hat{V}_2' + \hat{V}_1'\hat{V}_2', \tag{11}$$

where $\hat{O}$ and $\hat{V}$ project onto the set of occupied and virtual HF spin-orbitals, respectively. $\hat{V}'$ projects onto the space of CA orbitals and $\hat{V}'' = \hat{V} + \hat{V}'$ onto the full set of virtuals, that is, the HF virtuals and the CA orbitals.

The second- and third-order Møller–Plesset energy corrections are given by, respectively,

$$E_{\text{MP2-F12}} = \min L_{\text{MP2-F12}}, \tag{12}$$

with the Hylleraas functional

$$\begin{aligned} L_{\text{MP2-F12}} = &\sum_{i>j}\sum_{a>b} t_{ab}^{ij}\langle {}_{ab}^{ij}|[\hat{F}, \hat{T}_2 + \hat{T}_{2'}] + 2(\hat{H} - \hat{F})|\text{HF}\rangle \\ &+ \sum_{i>j}\sum_{x>y} c_{xy}^{ij}\langle {}_{xy}^{ij}|[\hat{F}, \hat{T}_2 + \hat{T}_{2'}] + 2(\hat{H} - \hat{F})|\text{HF}\rangle \end{aligned} \tag{13}$$

and

$$\begin{aligned} E_{\text{MP3-F12}} = &\sum_{i>j}\sum_{a>b} t_{ab}^{ij}\langle {}_{ab}^{ij}|[\hat{H} - \hat{F}, \hat{T}_2 + \hat{T}_{2'}]|\text{HF}\rangle \\ &+ \sum_{i>j}\sum_{x>y} c_{xy}^{ij}\langle {}_{xy}^{ij}|[\hat{H} - \hat{F}, \hat{T}_2 + \hat{T}_{2'}]|\text{HF}\rangle. \end{aligned} \tag{14}$$

In these equations t_{ab}^{ij} are the first-order double excitation amplitudes obtained by minimizing $L_{\text{MP2-F12}}$ and $c_{xy}^{ij} = \delta_{xy}^{ij} - \delta_{xy}^{ji}$ when the fixed amplitude (rational generator) (Ref. 40) approach is adopted. MP3-F12, like CCSD-F12, is an expensive and inefficient method. We therefore introduce the MP3(F12) approximation, which by analogy to CCSD(F12),[43] neglects contributions quadratic in the geminals and higher than second order in the electron fluctuation potential:

$$\begin{aligned} E_{\text{MP3(F12)}} = &\sum_{i>j}\sum_{a>b} t_{ab}^{ij}\langle {}_{ab}^{ij}|[\hat{H} - \hat{F}, \hat{T}_2 + \hat{T}_{2'}]|\text{HF}\rangle \\ &+ \sum_{i>j}\sum_{x>j} c_{xy}^{ij}\langle {}_{xy}^{ij}|[\hat{H} - \hat{F}, \hat{T}_2]|\text{HF}\rangle \end{aligned} \tag{15}$$

$$= \sum_{i>j}\sum_{a>b} t_{ab}^{ij}\langle {}_{ab}^{ij}|[\hat{H} - \hat{F}, \hat{T}_2 + 2\hat{T}_{2'}]|\text{HF}\rangle. \tag{16}$$

CCSD(F12) is an excellent approximation to CCSD-F12 due to a reliable near cancellation of the neglected third-order ring and ladder diagrams.[44] This same cancellation applies to MP3(F12), which is expected to be an equally excellent approximation to MP3-F12. We also note that the recently introduced approximations[45] CCSD(F12*) and CCSD[F12] are identical to CCSD(F12) up to third order so that all three approximate Lagrangians lead to the same MP3(F12) expressions.

Adopting the notation introduced in Ref. 45 for the explicitly correlated contributions, the MP3(F12) energy is

$$E_{\text{MP3(F12)}} = \sum_{i>j}\sum_{a>b} t_{ab}^{ij}\left(U_{ab}^{ij} + V_{ab}^{ij} + W_{ab}^{ij} + 2\mathcal{U}_{ab}^{ij} + 2\mathcal{V}_{ab}^{ij}\right) \tag{17}$$

with the conventional and F12 intermediates:

$$U_{ab}^{ij} = \hat{P}_{ab}\hat{P}_{ij}\sum_{kc} g_{ak}^{ic} t_{cb}^{kj}, \tag{18}$$

$$\mathcal{U}_{ab}^{ij} = \hat{P}_{ab}\hat{P}_{ij}\sum_{kc'} g_{ak}^{ic'} r_{c'b}^{kj}, \tag{19}$$

$$V_{ab}^{ij} = \sum_{c>d} g_{ab}^{cd} t_{cd}^{ij}, \tag{20}$$

$$\mathcal{V}_{ab}^{ij} = v_{ab}^{ij} - \sum_{c>d} g_{ab}^{cd} r_{cd}^{ij} - \sum_{K>L} g_{ab}^{KL} r_{KL}^{ij} - \sum_{Kc''} g_{ab}^{Kc''} r_{Kc''}^{ij}, \tag{21}$$

$$W_{ab}^{ij} = \sum_{k>l} g_{kl}^{ij} t_{ab}^{kl}. \tag{22}$$

Above, $\hat{P}_{ab}$ and $\hat{P}_{ij}$ are antisymmetrisation operators defined by $\hat{P}_{pq}X_{pq} = X_{pq} - X_{qp}$ and $g_{rs}^{pq} = \langle pq||rs\rangle$ are antisymmetrised electron repulsion integrals. $r_{pq}^{ij} = \langle pq|f(r_{12})|\widetilde{ij}\rangle$ and $v_{ab}^{ij} = \langle ab|r_{12}^{-1}f(r_{12})|\widetilde{ij}\rangle$ with $|\widetilde{ij}\rangle = \hat{P}_{ij}\left(\frac{3}{8} + \frac{1}{8}\hat{S}_{ij}\right)|\phi_i(1)\phi_j(2)\rangle$. The indices c' denote the auxiliary orbitals used to span the complementary virtual subspace in the projector $\hat{V}'$ and with c'' we indicate orbitals from the union of the virtual (c) and the complementary virtual (c') space. Capital letters K, L are used to denote all (i.e., frozen and active) occupied orbitals. In the MP3(F12) energy terms, $^{B}\hat{Q}_{12}$ has been used in the evaluation of $\mathcal{U}$ and $^{A}\hat{Q}_{12}$ for $\mathcal{V}$. For the MP2-F12 energy expressions we refer the reader to the extensive literature.[17,18,46–48]

III. OSVs AND V-PNOs

A. Standard V-PNOs and OSVs

Our previous work followed Meyer, where we defined the set of virtual PNOs (V-PNOs) $\bar{a}_{ij}$ for an occupied pair ij as eigenvectors of a pseudo density $\mathbf{D}^{ij}$. If no F12 terms are included in the wave function parameterisation, then in the spin-orbital formalism

$$D_{ab}^{ij} = \sum_{c} t_{ac}^{ij} t_{bc}^{ij}, \tag{23}$$

Downloaded 24 May 2012 to 134.147.252.238. Redistribution subject to AIP license or copyright; see http://jcp.aip.org/about/rights_and_permissions

where the amplitudes t_{ab}^{ij} are approximate first-order amplitudes

$$t_{ab}^{ij} = -\frac{g_{ab}^{ij}}{\varepsilon_a + \varepsilon_b - F_{ii} - F_{jj}}. \tag{24}$$

F_{ii} are diagonal Fock matrix elements and ε_a are the orbital eigenvalues of the canonical virtual spin-orbitals. This differs from Meyer's definition in that we have dropped the normalisation factor. Even for strongly multireference cases where the amplitudes are large, the normalisation has a negligible effect on the calculation. Without the normalisation, the eigenvalues of $\mathbf{D}^{ij}$ are the singular values of the amplitudes and this seems a more natural choice. The set of PNOs $\bar{a}_{ij}$ used to correlate an orbital pair ij are selected to be the eigenvectors of $\mathbf{D}^{ij}$ with eigenvalues larger than a chosen threshold.

We define OSVs $\bar{a}_i$ for orbital i as the eigenvectors of a pseudo density $\mathbf{D}^{ii}$

$$D_{ab}^{ii} = \sum_c t_{ac}^{ii} t_{bc}^{ii}, \tag{25}$$

$$t_{ab}^{ii} = -\frac{K_{ab}^{ii}}{\varepsilon_a + \varepsilon_b - 2F_{ii}}, \tag{26}$$

with the exchange integral $K_{ab}^{ij} = \langle ij|ab\rangle$ and $g_{ab}^{ij} = K_{ab}^{ij} - K_{ba}^{ij}$. The OSVs for i are identical to the V-PNOs for the diagonal pair ii in a spin-free formulation. In a spin-orbital formulation, they have no well-founded physical meaning and should be understood merely as an auxiliary quantity for generating a localised orbital specific virtual basis.

B. V-PNOs and OSVs in F12 Theory

For explicitly correlated methods, a modified definition of V-PNOs is needed. We previously defined a pseudo pair difference density from difference amplitudes

$$D_{ab}^{ij} = \sum_c d_{ac}^{ij} d_{bc}^{ij}, \tag{27}$$

$$d_{ab}^{ij} = t_{ab}^{ij} - r_{ab}^{ij}. \tag{28}$$

The difference amplitudes are required because we are interested in finding a compact representation for the part of t_{ab}^{ij} that is not already captured by the geminal basis. In fact, inserting $t_{ab}^{ij} = d_{ab}^{ij} + r_{ab}^{ij}$ into the MP2-F12 Hylleraas functional and solving for d_{ab}^{ij} leads to a refined definition of the difference amplitudes

$$d_{ab}^{ij} = t_{ab}^{ij} - r_{ab}^{ij} - \frac{C_{ab}^{ij}}{\varepsilon_a + \varepsilon_b - F_{ii} - F_{jj}}, \tag{29}$$

where C_{ab}^{ij} is the matrix element $\langle ab|(\hat{F}_1 + \hat{F}_2)^B \hat{Q}_{12} f(r_{12})|\widetilde{ij}\rangle$. This additional coupling term is zero under the extended Brillouin condition. The refined difference amplitudes lead to a further reduction in the number of PNOs required for a given accuracy of the pair correlation functions. We adopted this refined method in the present work. For a thorough discussion of PNOs for F12 methods, the dependence of the results on the exponent and length-scale parameter γ in the correlation factor and an evaluation of the truncation thresholds for the pair-specific virtual and auxiliary basis sets we refer to Refs. 34 and 49.

We define OSVs for orbital i as the eigenvectors of a pseudo density $\mathbf{D}^{ii}$

$$D_{ab}^{ii} = \sum_c d_{ac}^{ii} d_{bc}^{ii}, \tag{30}$$

$$d_{ab}^{ii} = t_{ab}^{ii} - r_{ab}^{ii} - \frac{C_{ab}^{ii}}{\varepsilon_a + \varepsilon_b - 2F_{ii}}, \tag{31}$$

$$r_{ab}^{ii} = \tfrac{1}{2}\langle ab|f(r_{12})|ii\rangle, \tag{32}$$

$$C_{ab}^{ii} = \tfrac{1}{2}\langle ab|(\hat{F}_1 + \hat{F}_2)^B \hat{Q}_{12} f(r_{12})|ii\rangle. \tag{33}$$

IV. OSXs AND X-PNOs

Transforming the virtual orbitals to OSVs or PNOs ensures that the number of correlating orbitals for each pair is independent of system size. In explicitly correlated methods, the working equations involve auxiliary orbitals, arising from the RI insertions implicit in the approximation of the strong orthogonality projector. OSXs are orbital specific auxiliary orbitals and X-PNOs are pair specific auxiliary orbitals. Transforming to the OSX or X-PNO basis is necessary to ensure that the number of auxiliary orbitals in the working equations is independent of system size.

Several choices of X-PNOs are possible and these have been the subject of a recent article,[49] which concludes that the best choices for approximating the strong orthogonality operator in PNO theory are

$${}^A\hat{Q}_{ij} = 1 - \bar{\bar{O}}_1\bar{\bar{O}}_2 - \bar{V}_1\bar{V}_2 - \bar{O}_1 V_2'' - V_1''\bar{O}_2, \tag{34}$$

$${}^B\hat{Q}_{ij} = \bar{V}_1\bar{V}_2' + \bar{V}_1'\bar{V}_2 + \bar{V}_1'\bar{V}_2', \tag{35}$$

where

$$\bar{\bar{O}} = \sum_{\bar{\bar{K}}_{ij}} |\bar{\bar{K}}_{ij}\rangle\langle\bar{\bar{K}}_{ij}|, \tag{36}$$

$$\bar{O} = \sum_{\bar{K}_{ij}} |\bar{K}_{ij}\rangle\langle\bar{K}_{ij}|, \tag{37}$$

$$\bar{V} = \sum_{\bar{a}_{ij}} |\bar{a}_{ij}\rangle\langle\bar{a}_{ij}|, \tag{38}$$

$$\bar{V}' = \sum_{\bar{a}'_{ij}} |\bar{a}'_{ij}\rangle\langle\bar{a}'_{ij}|. \tag{39}$$

Downloaded 24 May 2012 to 134.147.252.238. Redistribution subject to AIP license or copyright; see http://jcp.aip.org/about/rights_and_permissions

A. X-PNOs

The X-PNOs are defined by the pseudo pair densities that they diagonalise

$$\bar{\bar{K}}_{ij}: \qquad \bar{\bar{D}}^{ij}_{KL} = \sum_{M} r^{ij}_{KM} r^{ij}_{LM}, \tag{40}$$

$$\bar{K}_{ij}: \qquad \bar{D}^{ij}_{KL} = \sum_{c''} r^{ij}_{Kc''} r^{ij}_{Lc''}, \tag{41}$$

$$\bar{a}'_{ij}: \qquad \bar{D}^{ij}_{a'_{ij}b'_{ij}} = \sum_{\bar{c}_{ij}} r^{ij}_{a'_{ij}\bar{c}_{ij}} r^{ij}_{b'_{ij}\bar{c}_{ij}}. \tag{42}$$

The orbitals a'_{ij} span the union of the CA orbitals a' and the set of V-PNOs that are discarded from the space of orbitals used to correlate pair ij. In Ref. 49 we demonstrated that the occupation number threshold $T_{\text{X-PNO}}$ for the X-PNOs can be related straightforwardly to that of the V-PNOs, denoted by T_{PNO}, such that the error incurred by truncating the auxiliary basis is at least an order of magnitude smaller than the error incurred by truncating the virtual basis, even for energy differences. Specifically, $-\log_{10} T_{\text{X-PNO}} = 5.5 - 0.5 \log_{10} T_{\text{PNO}}$ for $\bar{\bar{K}}_{ij}$ and $\bar{K}_{ij}$ and $-\log_{10} T_{\text{X-PNO}} = 0.5 - \log_{10} T_{\text{PNO}}$ for $\bar{a}'_{ij}$.

B. OSXs

The OSXs are likewise defined by the pseudo pair densities that they diagonalise

$$\bar{\bar{K}}_{i}: \qquad \bar{\bar{D}}^{ii}_{KL} = \sum_{M} r^{ii}_{KM} r^{ii}_{LM}, \tag{43}$$

$$\bar{K}_{i}: \qquad \bar{D}^{ii}_{KL} = \sum_{p''} r^{ii}_{Kp''} r^{ii}_{Lp''}, \tag{44}$$

$$\bar{a}''_{i}: \qquad \bar{D}^{ii}_{a''b''} = \sum_{c''} r^{ii}_{a''c''} r^{ii}_{b''c''}, \tag{45}$$

where p'' runs over the whole unified HF and CA orbital basis. Some comments are required regarding the above definitions. The OSXs should provide accurate approximations to the integrals r^{ij}_{KL}, $r^{ij}_{Kc''}$, and $r^{ij}_{a'b}$. Taking first r^{ij}_{KL} as an example, diagonalising $\bar{\bar{D}}^{ii}_{KL}$ for each i ensures that each discarded integral $r^{ii}_{\bar{\bar{K}}_i \bar{\bar{K}}_i}$ in the OSX basis is smaller than a given threshold, which by Schwartz's inequality ensures that each discarded integral in $\langle \bar{\bar{K}}_i \bar{\bar{L}}_j | f(r_{12}) | ij \rangle$ is smaller than the threshold. To accurately represent r^{ij}_{KL} we additionally require that $\langle KL | f(r_{12}) | ji \rangle$ is well represented, which can be achieved by merging the OSXs $\bar{\bar{K}}_i$ and $\bar{\bar{K}}_j$.

Consider now the integral $r^{ij}_{Kc''}$. If one diagonalised $\sum_{c''} r^{ii}_{Kc''} r^{ii}_{Lc''}$, this would only ensure that the integrals $r^{ii}_{Kc''}$ are well represented. For an accurate description of $\langle Kc'' | f(r_{12}) | ij \rangle$, Schwartz's inequality dictates that we require an accurate representation of both r^{ii}_{KK} and $r^{ii}_{c''c''}$. This is why $\bar{\bar{D}}^{ii}_{KL}$ is defined using p'', which is the union of K and c''.

V. OSV-PNO-MP3 THEORY

A. OSVs as pre-PNOs

To perform a PNO calculation one must first construct the pair-specific natural orbitals from approximate double excitation amplitudes t^{ij}_{ab} through a singular value decomposition or the diagonalisation of (pseudo) pair densities. It is common practice to preselect the set of non-negligible pairs ij based on pair energy estimates, also from t^{ij}_{ab}. Most of the recently reported implementations[30,36,50] use for these initial steps approximate RI-MP2 amplitudes, where off-diagonal Fock matrix elements F_{ij} are neglected. Without *a priori* truncation of the pair list, the virtual space, or the auxiliary density-fitting basis, the computational costs for the calculation of the amplitudes and pair energy estimates scale as $\mathcal{O}(O^2V^2N_X)$. Subsequent diagonalisation of the densities for the selected non-negligible pairs scales as $\mathcal{O}(N_p V^3)$. O, V, N_X, and N_p are the numbers of occupied, virtual, and auxiliary orbitals and the number of non-negligible pairs, respectively. Even though (canonical) RI-MP2 calculations are today possible on rather large molecules, the steep scaling currently limits routine applications of PNO-based methods to systems not much larger than about hundred atoms.

An evident possibility to reduce the computational costs for the construction of PNOs, without digressing from the strategy to determine pair-specific optimised virtual spaces from approximate doubles amplitudes, is to adopt a hybrid OSV-PNO approach. In an initial step the OSVs are determined as eigenvectors of the pseudo densities for diagonal pairs:

$$D^{ii}_{ab} L^{\bar{a}_i}_{b} = n_{\bar{a}_i} L^{\bar{a}_i}_{a}, \tag{46}$$

where i is a localised occupied and a, b are canonical virtual orbitals and D^{ii}_{ab} is given in Eq. (25). The integrals K^{ii}_{ab}, required for D^{ii}_{ab}, are evaluated using the resolution-of-the-identity (RI) or density-fitting (DF) approximation from three-index intermediates:

$$K^{ii}_{ab} = \sum_{Q} B_{Q,ai} B_{Q,bi}, \tag{47}$$

$$B_{Q,ai} = \sum_{P} [\mathbf{V}^{-1/2}]_{QP} (Q|ai), \tag{48}$$

where $(Q|ai)$ are three-index and $V_{PQ} = (P|Q)$ are two-index electron repulsion integrals (ERIs), and P, Q are density-fitting auxiliary functions. With this, the computation of the OSVs displays an $\mathcal{O}(ON^3)$ scaling without integral screening or local restrictions of the DF auxiliary basis. The number of OSVs for an orbital i with eigenvalues $n_{\bar{a}_i}$ below a given threshold T_{OSV} is independent of the system size.

Once the OSVs have been obtained for all occupied orbitals, the intermediates $B_{Q,ai}$ can be transformed to the OSV basis of the respective occupied orbital i and combined to the exchange integrals $K^{ij}_{\bar{a}_i \bar{b}_j}$ with $\mathcal{O}(\mathcal{N}^3)$ costs. These integrals are well suited to evaluate the Coulomb contribution to the pair correlation energy of pair ij, but less appropriate for the exchange correlation contribution. We can, however, exploit that the Coulomb contribution, which is the only contribution kept in the scaled opposite spin (SOS) variant

Downloaded 24 May 2012 to 134.147.252.238. Redistribution subject to AIP license or copyright; see http://jcp.aip.org/about/rights_and_permissions

of MP2, is closely correlated with the total pair contribution to the second-order correlation energy and calculate a correlation energy importance diagnostic for each pair as

$$e_{ij}^{\text{est}} = \frac{c_{OS}}{2} \sum_{\bar{a}_i \bar{b}_j} \frac{\left(K_{\bar{a}_i \bar{b}_j}^{ij}\right)^2}{F_{ii} - F_{\bar{a}_i \bar{a}_i} + F_{jj} - F_{\bar{b}_j \bar{b}_j}}. \tag{49}$$

We find that with $c_{OS} = 1.5$ these estimates agree typically within a factor of 2 with pair energy estimates obtained as suggested, e.g., in Ref. 30 from the approximate RI-MP2 amplitudes (without OSV truncation) and used in our initial PNO-MP2-F12 implementation.[34]

Pairs with e_{ij}^{est} below a certain threshold T_{pair} can at this point be discarded and the number of pairs retained scales linearly with system size. If T_{pair} is set such that only pairs are discarded which cannot have PNOs with eigenvalues above T_{PNO} this truncation does not affect the final results. For the remaining pairs ij, PNOs can be formed using the OSVs for orbitals i and j. First, the OSV spaces for orbitals i and j are unified and transformed to an orthonormal and quasicanonical pre-PNO basis $\tilde{a}_{ij}$ with $F_{\tilde{a}_{ij},\tilde{b}_{ij}} = \delta_{\tilde{a}_{ij},\tilde{b}_{ij}} \varepsilon_{\tilde{a}_{ij}}$. In this basis, the exchange integrals, guess amplitudes, pair densities, and PNO coefficients are all evaluated in the same way as for the original PNO approaches in the full canonical virtual basis:

$$t_{\tilde{a}_{ij}\tilde{b}_{ij}}^{ij} = \frac{K_{\tilde{a}_{ij}\tilde{b}_{ij}}^{ij} - K_{\tilde{b}_{ij}\tilde{a}_{ij}}^{ij}}{F_{ii} - \varepsilon_{\tilde{a}_{ij}} + F_{jj} - \varepsilon_{\tilde{b}_{ij}}}, \tag{50}$$

$$D_{\tilde{a}_{ij}\tilde{b}_{ij}}^{ij} = \sum_{\tilde{c}_{ij}} t_{\tilde{a}_{ij}\tilde{c}_{ij}}^{ij} t_{\tilde{b}_{ij}\tilde{c}_{ij}}^{ij}, \tag{51}$$

$$\sum_{\tilde{b}_{ij}} D_{\tilde{a}_{ij}\tilde{b}_{ij}}^{ij} L_{\tilde{b}_{ij}}^{\bar{b}_{ij}} = n_{\bar{a}_{ij}} L_{\tilde{a}_{ij}}^{\bar{a}_{ij}}. \tag{52}$$

In the regime of a linearly scaling number of non-negligible pairs ij, the costs for the evaluation of the integrals $K_{\tilde{b}_{ij}\tilde{a}_{ij}}^{ij}$ scale quadratically with system size. The cost of building and diagonalising the pseudo pair densities scales linearly with system size and also the exchange integrals in the PNO basis can be obtained from those in the pre-PNO basis with this scaling.

In summary, the above algorithm scales only with the fourth power of system size for the construction of the PNO basis and the exchange integrals needed to solve the equations for the first-order amplitudes. This is the same scaling as for the OSV-MP2 algorithms reported by Yang *et al.*,[36] but as pointed out in the introduction, the PNO basis gives a very substantial reduction of the number of doubles amplitudes which have to be stored and processed. This reduces the costs in particular for MP3 and higher order methods.

B. Local MP3 with pair natural orbitals

The expressions for the PNO-MP3 energy correction and the PNO analogues of the intermediates U_{ab}^{ij}, V_{ab}^{ij}, and W_{ab}^{ij} defined in Eqs. (18), (20), and (22) are obtained by projecting the doubles amplitudes onto the virtual PNO subspace for every pair ij. With this, we obtain for the PNO-MP3 energy:

$$E_{\text{PNO-MP3}} = \sum_{i>j} \sum_{\bar{a}>\bar{b}} t_{\bar{a}\bar{b}}^{ij} \left(U_{\bar{a}\bar{b}}^{ij} + V_{\bar{a}\bar{b}}^{ij} + W_{\bar{a}\bar{b}}^{ij}\right). \tag{53}$$

To make the presentation of the implementation simpler, we introduce the shorthand notation $J_{ab}^{ij} = \langle ia|jb\rangle$ and $K_{ab}^{ij} = \langle ij|ab\rangle$. Note that these integrals are not antisymmetrised. With this notation we can write the intermediates as:

$$U_{\bar{a}\bar{b}}^{ij} = \hat{P}_{\bar{a}\bar{b}} \hat{P}_{ij} \sum_{k\bar{c}_{jk}} \left(K_{\bar{a}_{ij}\bar{c}_{jk}}^{ik} - J_{\bar{a}_{ij}\bar{c}_{jk}}^{ik}\right) t_{\bar{c}\bar{b}}^{kj} S_{\bar{b}_{kj}\bar{b}_{ij}}^{kj,ij}, \tag{54}$$

$$V_{\bar{a}\bar{b}}^{ij} = \sum_{\bar{c}>\bar{d}} g_{\bar{a}\bar{b}}^{\bar{c}\bar{d}} t_{\bar{c}\bar{d}}^{ij}, \tag{55}$$

$$W_{\bar{a}\bar{b}}^{ij} = \sum_{k>l} \sum_{\bar{a}_{kl}} S_{\bar{a}_{ij}\bar{a}_{kl}}^{ij,kl} \sum_{\bar{b}_{kl}} S_{\bar{b}_{ij}\bar{b}_{kl}}^{ij,kl} g_{kl}^{ij} t_{\bar{a}\bar{b}}^{kl}. \tag{56}$$

For notational convenience we have dropped the pair index on the PNO orbitals when it is identical with the pair index of the amplitudes or the intermediate. $S^{ij,kl}$ are PNO overlap matrices defined as

$$S_{\bar{a}_{ij}\bar{b}_{kl}}^{ij,kl} = \sum_{c} L_c^{\bar{a}_{ij}} L_c^{\bar{b}_{kl}}. \tag{57}$$

Our implementation relies upon the resolution-of-the-identity (RI) or density-fitting (DF) approximation for the two-electron integrals. To evaluate U we start with the computation of the three-index ERIs $(Q|\mu k) = \sum_\nu (Q|\mu\nu) C_{\nu k}$ and $(Q|ik) = \sum_\mu (Q|\mu k) C_{\mu i}$, where μ, ν are atomic orbitals (AOs) and Q are the density-fitting auxiliary functions. These steps have quartic or lower cost scalings with low prefactors and contribute little to the overall timing. From these three-index integrals we form in a second step the Coulomb and exchange matrices:

$$J_{\mu\nu}^{ik} = \sum_{QP} (\mu\nu|P) [\mathbf{V}^{-1}]_{PQ} (Q|ik), \tag{58}$$

$$K_{\mu\nu}^{ik} = \sum_{QP} (\mu i|P) [\mathbf{V}^{-1}]_{PQ} (Q|\nu k). \tag{59}$$

In a loop over the non-negligible triples of occupied orbitals, the Coulomb and exchange matrices are transformed from the AO to the PNO basis, contracted with the amplitudes and then transformed using the overlap matrices $S_{\bar{b}_{kj}\bar{b}_{ij}}^{kj,ij}$ into the PNO basis of the target pair ij. For large molecules the number of occupied orbitals k interacting with a given pair ij becomes independent of the system size and the cost scaling for the intermediate U becomes then quadratic.

To evaluate $V_{\bar{a}\bar{b}}^{ij}$ we compute the ERIs in a loop over the non-negligible pairs ij. In a first step we evaluate the partially transformed three-index ERIs $(Q|\mu\bar{a}_{ij}) = \sum_\nu (Q|\mu\nu) C_{\nu\bar{a}_{ij}}$ from which we then calculate $(Q|\bar{b}_{ij}\bar{a}_{ij})$. In a next step the three-index intermediates are transformed with $\mathbf{V}^{-1}$ and combined to four-index electron repulsion integrals, which are then contracted with the first-order amplitudes. Transforming in the first half-transformation only the significant three-index integrals not discarded by the Schwartz screening leads for this and the following transformation steps to a cubic cost

Downloaded 24 May 2012 to 134.147.252.238. Redistribution subject to AIP license or copyright; see http://jcp.aip.org/about/rights_and_permissions

scaling. The prefactors are, however, rather large and increase rapidly with the number of PNOs kept per pair. To reduce the costs further, we use for the evaluation of the intermediate $V^{ij}_{\bar{a}\bar{b}}$ a pair-specific truncation of the density-fitting basis, similar to that used in domain-based local correlation methods[9] and in the LPNO-CEPA implementation reported in Ref. 30, but with a threshold which is determined for each pair such that the errors are insignificant within a user-specified error tolerance.

Finally, the intermediate $W^{ij}_{\bar{a}\bar{b}}$ is evaluated in a manner similar to that described in Ref. 30. For large molecules the number of pairs kl with non-negligible overlap matrix elements $S^{ij,\,kl}$ with a given pair ij becomes independent of the system size. The computation of the overlap matrix elements $S^{ij,\,kl}$ and the integrals g^{ij}_{kl} scale quadratically and the subsequent contractions to form $W^{ij}_{\bar{a}\bar{b}}$ linearly with system size.

VI. OSV-PNO-MP3(F12) THEORY

A. OSXs as pre-X-PNOs

In the same way that OSVs can be used as pre-V-PNOs, OSXs can be used as pre-X-PNOs. Taking the X-PNOs $\bar{a}'_{ij}$ as an example, first the set of OSXs $\bar{a}''_i$ are computed by diagonalising $\bar{D}^{ii}_{a''b''}$ in Eq. (45). This step scales as $\mathcal{O}(ON^2N_X)$ at worst and the number of OSXs $\bar{a}''_i$ with eigenvalues above a given tolerance is independent of system size. For every non-negligible pair ij a set of orthonormal orbitals $\tilde{a}'_{ij}$ are formed from the union of $L^{\bar{a}''_i}_{a''}$ and $L^{\bar{a}''_j}_{a''}$. Then, finally, the X-PNOs are computed as the eigenvectors of

$$\bar{D}^{ij}_{\bar{a}'_{ij}\bar{b}'_{ij}} = \sum_{\bar{c}_{ij}} r^{ij}_{\bar{a}'_{ij}\bar{c}_{ij}} r^{ij}_{\bar{b}'_{ij}\bar{c}_{ij}}. \tag{60}$$

Without the pre-X-PNOs, this step scaled as $\mathcal{O}(N_pVNN_X)$ and $\mathcal{O}(N_pN^3)$. Using the OSXs as pre-X-PNOs reduces this to a cubically scaling step. While the overall scaling with system size for the cost of construction of the X-PNOs is $\mathcal{O}(\mathcal{N}^4)$ with or without pre-PNOs, the prefactor is much smaller when pre-X-PNOs are used and the $\mathcal{O}(\mathcal{N}^4)$ scaling is seen already for much smaller system sizes.

B. Local MP3(F12) with pair natural orbitals

The expressions for the PNO analogues of $\mathcal{U}^{ij}_{ab}$ and $\mathcal{V}^{ij}_{ab}$ in Eqs. (19) and (21) are obtained by projecting the doubles amplitudes onto the virtual PNO subspace for every pair ij and also projecting the indices K, L, and c' or c'' onto the X-PNOs:

$$\mathcal{U}^{ij}_{\bar{a}\bar{b}} = \hat{P}_{\bar{a}\bar{b}}\hat{P}_{ij}\sum_{kc'}\left(K^{ik}_{\bar{a}_{ij}\bar{c}'_{jk}} - J^{ik}_{\bar{a}_{ij}\bar{c}'_{jk}}\right) r^{kj}_{\bar{c}'_{kj}\bar{b}_{kj}} S^{kj,ij}_{\bar{b}_{kj}\bar{b}_{ij}}, \tag{61}$$

$$\mathcal{V}^{ij}_{\bar{a}\bar{b}} = v^{ij}_{\bar{a}\bar{b}} - \sum_{\bar{c}>\bar{d}} g^{\bar{c}\bar{d}}_{\bar{a}\bar{b}} r^{ij}_{\bar{c}\bar{d}} - \sum_{\bar{\bar{K}}>\bar{\bar{L}}} g^{\bar{\bar{K}}\bar{\bar{L}}}_{\bar{a}\bar{b}} r^{ij}_{\bar{\bar{K}}\bar{\bar{L}}} - \sum_{\bar{K}\bar{c}''} g^{\bar{K}\bar{c}''}_{\bar{a}\bar{b}} r^{ij}_{\bar{K}\bar{c}''}. \tag{62}$$

Comparing Eqs. (61) and (62) with Eqs. (54) and (55), it is obvious that the F12 intermediates $\mathcal{U}$ and $\mathcal{V}$ can be evaluated using similar computational strategies to their conventional counterparts. However, several additional integrals are required to evaluate $\mathcal{V}$ and $\mathcal{U}$. All integrals over $f(r_{12})$ are computed at the same time as the MP2-F12 energy and are stored on disk in their PNO representation. The integrals $(Q|\bar{\bar{K}}_{ij}\bar{a}_{ij})$ required for $g^{\bar{\bar{K}}\bar{\bar{L}}}_{\bar{a}\bar{b}}$ are obtained together with $(Q|\bar{K}_{ij}\bar{a}_{ij})$ from the partially transformed three-index ERIs $(Q|\mu\bar{a}_{ij})$ which are used to construct V. The final contribution is computed as

$$A^{ij}_{Q,\bar{K},\bar{a}} = \sum_{\mu}(Q|\mu\bar{a}_{ij})\sum_{c'} r^{ij}_{\bar{K}c''} C_{\mu c''}, \tag{63}$$

$$\sum_{\bar{K}\bar{c}''} g^{\bar{K}\bar{c}''}_{\bar{a}\bar{b}} r^{ij}_{\bar{K}\bar{c}''} = \sum_{\bar{K},P} A^{ij}_{P,\bar{K},\bar{b}} \sum_{Q}[V^{-1}]_{PQ}(Q|\bar{K}_{ij}\bar{a}_{ij}). \tag{64}$$

First the intermediate $A^{ij}_{Q,\bar{K},\bar{a}}$ is computed where the F12 integrals act as an orbital transformation. This is then transformed with $\mathbf{V}^{-1}$ and combined with the electron repulsion integrals. As for its conventional counterpart, we use also for $\mathcal{V}$ a pair-specific truncation of the density-fitting basis.

The costs for the individual steps in the computation of the $\mathcal{V}$ and $\mathcal{U}$ intermediates scale as for their conventional counterparts at worst cubically with the system size. Since the CABS orbitals c' are expanded in the union of the usual AO and the auxiliary AO basis set and because of the larger number of contributions to $\mathcal{V}$, the prefactors are larger than for the conventional intermediates. But this is also the case in canonical implementations.

VII. RESULTS AND DISCUSSION

A. Performance of the hybrid OSV-PNO approach for MP2 and MP3

To test the performance of the OSV-PNO approach in terms of accuracy and computational time, we carried out a series of MP2 calculations on $(\text{glycine})_n$ polypeptides with the RI-MP2, PNO-MP2, and OSV-PNO-MP2 methods. The OSV-PNO- and PNO-MP2 calculations have been performed using the PNO code described above and in Refs. 34, 35, and 49, which is part of a development version of the TURBOMOLE package.[51] The HF-SCF and RI-MP2 calculations were performed using the dscf (Ref. 52) and ricc2 programs[53] from the TURBOMOLE V6.3 release.[54] All MP2 calculations use the optimised DF auxiliary basis sets reported in Ref. 55.

Fig. 1 shows a comparison of the PNO and combined OSV-PNO truncation errors in the MP2 correlation energy for glycine chains with 2, 4, and 8 units with the aug-cc-pVTZ (Refs. 56 and 57) basis set. For these calculations we have set the threshold for truncating the OSV space (T_{OSV}) to the same value as the PNO truncation threshold (T_{PNO}) to make the additional truncation error visible. Nevertheless, the results of the OSV-PNO-MP2 calculations are close to the PNO-MP2 results and the truncation errors vary little with the system size. For both approaches the relative errors in the MP2 energy converge with the same rate to zero, with the remaining error roughly proportional to the square root of T_{PNO}. However, we prefer to consider the OSVs merely as a numerical tool for accelerating the PNO calculation than an

Downloaded 24 May 2012 to 134.147.252.238. Redistribution subject to AIP license or copyright; see http://jcp.aip.org/about/rights_and_permissions

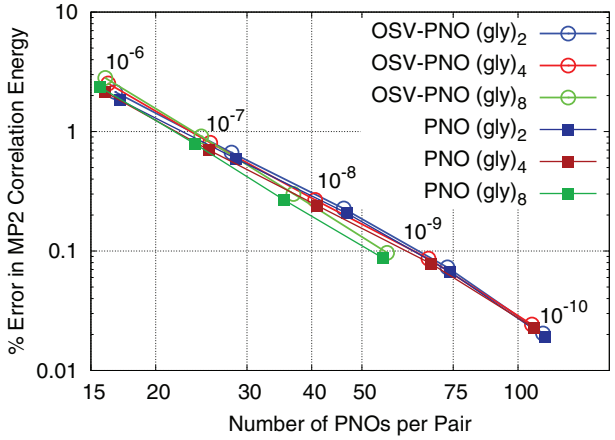


FIG. 1. Comparison of the truncation errors in the PNO and the OSV-PNO hybrid scheme for the MP2/aug-cc-pVTZ correlation energies of glycine chains with 2, 4, and 8 units with truncation thresholds between 10^{-6} and 10^{-10}.

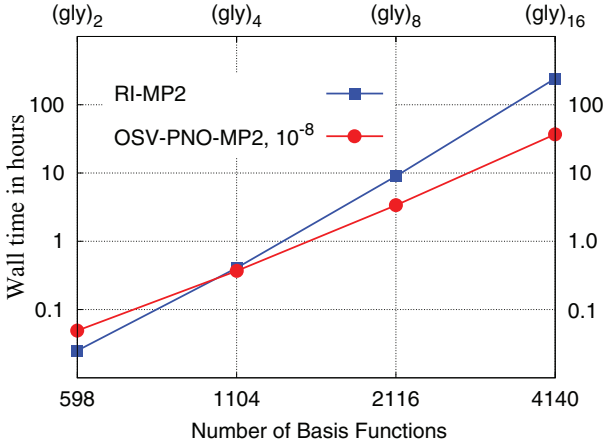


FIG. 2. Comparison of the wall clock time (in hours on an Intel Xeon E5430 2.66 GHz CPU) for canonical RI-MP2 and local OSV/PNO-MP2 calculations with the OSV and PNO truncation thresholds set to 10^{-8} for glycine chains with 2, 4, 8, and 16 units and the aug-cc-pVTZ basis sets.

additional degree of freedom for approximating the wavefunction expansion. The errors introduced by the OSV truncation should thus be at least an order of magnitude smaller than the PNO truncation errors. The results for the $(\text{glycine})_2$ dipeptide, listed in Table I, show that this criterion is safely met with $T_{\text{OSV}} = 0.1\,T_{\text{PNO}}$. If $T_{\text{OSV}} = T_{\text{PNO}}$ is chosen, the truncation errors for loose T_{PNO} are 10%–15% greater than we would like. In Table I we have also listed the percentage of the double excitation amplitudes kept for this example after OSV and after PNO truncation. For this molecule and basis set, the PNO truncation reduces the dimension of the double excitation space by a factor of 5–15 compared to its dimension after OSV truncation. This underlines the compactness of the PNO representation compared to OSVs.

Fig. 2 shows a comparison of the computational time for OSV-PNO-MP2 calculations on the glycine oligomers with the aug-cc-pVTZ basis and the truncation thresholds set to 10^{-8} with timings from canonical RI-MP2 calculations with the ricc2 program. This graph demonstrates the quartic scaling of the computational costs for OSV-PNO-MP2. Already with the present (still preliminary) implementation the break-even point with canonical RI-MP2 calculations is at about 1000 basis functions, where the calculations still take less than half an hour. Thus, calculations on systems of a size studied routinely with MP2 theory can already benefit from the computational savings. We also note that up to $(\text{glycine})_{16}$ the OSV-PNO-MP2 calculations are faster than the HF-SCF calculations, which were performed using TURBOMOLE's dscf program and started from an extended Hückel theory (EHT) guess for the molecular orbitals.

TABLE I. Truncation errors (Δ_{trunc} in mH/atom) for the MP2/aug-cc-pVTZ correlation energy of $(\text{glycine})_2$ for the PNO and hybrid OSV-PNO methods, with PNO thresholds between 10^{-6} and 10^{-10}. OSV-PNO-MP2 results are tabulated for initial OSV truncation with $T_{\text{OSV}} = T_{\text{PNO}}$ and with $T_{\text{OSV}} = 0.1 T_{\text{PNO}}$, for PNO-MP2 there is no initial OSV truncation. $\%T_{\text{OSV}}$ and $\%T_{\text{PNO}}$ are, respectively, the percentages of double excitation amplitudes kept after the OSV and the PNO truncation of the virtual space.

	$T_{\text{OSV}} = T_{\text{PNO}}$		$T_{\text{OSV}} = 0.1\,T_{\text{PNO}}$		PNO-MP2	
T_{PNO}	Δ_{trunc}	$\%T_{\text{OSV}}$	Δ_{trunc}	$\%T_{\text{OSV}}$	Δ_{trunc}	$\%T_{\text{PNO}}$
10^{-6}	2.5	1.5	2.2	3.5	2.1	0.1
10^{-7}	0.77	3.7	0.69	7.6	0.68	0.3
10^{-8}	0.26	7.8	0.24	15.4	0.24	1.0
10^{-9}	0.084	15.5	0.078	30.2	0.077	2.6
10^{-10}	0.023	30.2	0.022	50.2	0.022	6.0

Fig. 3 shows a similar summary of results from benchmark calculations with OSV-PNO-MP3 on the glycine polypeptides. The canonical MP3 calculations have been carried out with the CCSD implementation in the ricc2 program, discarding all fourth- and higher order terms. The PNO truncation errors have been determined by comparing with a test implementation which uses the density-fitting approximation for all ERIs. The truncation errors converge with a decreasing threshold T_{PNO} smoothly towards zero, just as they do for OSV-PNO-MP2. From the three contributions to the MP3 energy correction in Eq. (53) only the "ring diagram" contribution from the U intermediate is negative and the "ladder diagram" contributions from W and V are positive. They cancel to a large extend so that the sign of the total third-order correction depends on the balance between ring and ladder diagram contributions. Due to the presence of the fourfold external integrals g_{ab}^{cd} in the intermediate V, its contribution converges slowest with the one-electron basis set and also with the PNO truncation threshold. As a consequence, the overall truncation error in the third-order energy correction is typically about an order of magnitude smaller than the truncation error of the second-order energy and has the opposite sign. Due to this partial cancellation, the errors in the total PNO-MP3 correlation energy are slightly smaller than in $E_{\text{PNO-MP2}}$.

Not unexpectedly, we find for OSV-PNO-MP3 a much earlier break-even point of the computational time with the canonical implementation: in the cc-pVDZ basis[56,57] with $T_{\text{PNO}} = 10^{-8}$ the break-even point is met for the dipeptide. For the aug-cc-pVTZ basis and the same threshold, the calculation for the glycine monomer already shows a small speed up. The wall time for the OSV-PNO-MP3 calculations scales in this series as $\mathcal{O}(\mathcal{N}^3)$ with the system size, while for the

Downloaded 24 May 2012 to 134.147.252.238. Redistribution subject to AIP license or copyright; see http://jcp.aip.org/about/rights_and_permissions

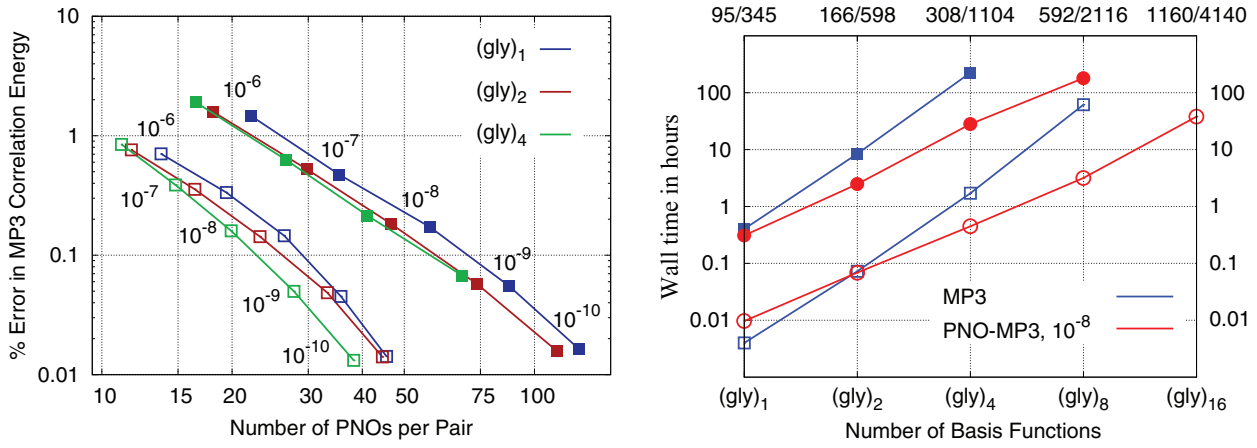


FIG. 3. Performance of the OSV-PNO-MP3 implementation. (Left) Convergence of the total MP3 correlation energy with the PNO truncation threshold for glycine chains with 1–4 units in the basis sets cc-pVDZ (□) and aug-cc-pVTZ (■). Results are shown for PNO truncation thresholds $-\log_{10} T_{\mathrm{PNO}} = 6$, 7, 8, 9, and 10 and OSV truncation threshold set to $0.1 \times T_{\mathrm{PNO}}$. (Right) Comparison of the wall clock time (in hours) for canonical MP3 and local OSV-PNO-MP3 calculations with the OSV and PNO truncation thresholds set to, respectively, 10^{-9} and 10^{-8} for glycine chains in the basis sets cc-pVDZ (open symbols, □ and ○) and aug-cc-pVTZ (filled symbols, ■ and ●).

canonical calculations we find a scaling with $\mathcal{O}(\mathcal{N}^{4.5})$ with, however, a smaller prefactor.

B. Performance of PNO-MP2-F12 and PNO-MP3(F12)

The explicitly correlated variants of MP2 and PNO-MP2 require the computation of several additional two-electron integrals beyond those of standard MP2 theory. In the canonical[48] as well as in the PNO implementation these integrals are evaluated with the DF approximation from two- and three-index integrals, so that the final assembly of the four-index integrals in the MO basis has a small prefactor. In Table II we have listed some results for MP2-F12 and MP3(F12) calculations on the glycine polypeptides with the aug-cc-pVDZ (Refs. 56 and 57) basis. We used for these calculations the optimised CA basis from Ref. 58 with an exponent of 1.0 for the Slater-type correlation factor and the aug-cc-pwCVTZ density-fitting basis.[59] Up to the tetrapeptide, the timings for MP2-F12 scale effectively as $\mathcal{N}^{3.94}$ with the number of correlated electrons and from the tetra- to the octapeptide with $\mathcal{N}^{4.32}$. This demonstrates the extent to which the $\mathcal{O}(\mathcal{N}^4)$ and lower scaling steps dominate the costs. For the OSV-PNO implementation of MP2-F12 we find in this regime effectively a scaling with $\mathcal{N}^{3.5}$. The computational savings compared to the canonical implementation are more pronounced in MP2-F12 due to the large prefactor for the integral evaluation. Although the reduction in effective scaling with the OSV-PNO implementation is less for MP2-F12 than for MP2, it has a very early onset: Already for the glycine monomer the OSV-PNO calculation is with $T_{\mathrm{PNO}} = 10^{-8}$ slightly faster than the canonical MP2-F12 calculation and for the tetrapeptide, which was the break-even point for MP2/aug-cc-pVTZ, we obtain for MP2-F12 a speed up of 1.7 and for the octapeptide already a speed up of 2.9. The findings for MP3(F12) are similar. The OSV-PNO calculation on the glycine molecule with $T_{\mathrm{PNO}} = 10^{-8}$ is slightly faster than the canonical calculation and one obtains already for medium-sized systems a significant speed-up. For the tetrapeptide (31 atoms, 517 basis functions) PNO-MP3(F12) is already more than three times faster than the canonical implementation.

TABLE II. Performance of the OSV-PNO implementation for MP2-F12 and MP3(F12) for glycine polypeptides. t_{can} and t_{PNO} are the wall clock timings for the canonical and OSV-PNO calculations (in min) on Intel Xeon E5430 2.66 GHz (MP2-F12) and Intel Xeon X5670 2.93 GHz (MP3(F12)), $\%_{corr}$ is the percentage of correlation energy lost in the OSV-PNO calculation, O_{core} and O_{act} are the number of frozen and active occupied, V is the number of virtual, and CABS is the number of complementary auxiliary orbitals. PNO is the average number of standard virtual PNOs per pair and OPNO-1 and OPNO-2 are the average number of OPNOs for, respectively, the $\bar{\bar{O}}\,\bar{\bar{O}}$ and $\bar{O}V''$ projectors. CAPNO-B is the average number of CA-PNOs for ${}^{B}\hat{Q}_{ij}$.

No.of glycines	T_{PNO}	O_{core}	O_{act}	OPNO-1	OPNO-2	V	PNO	CABS	CAPNO-B	N_{pair}	MP2-F12 $\%_{err}$	MP2-F12 t_{can}	MP2-F12 t_{PNO}	MP3(F12) $\%_{err}$	MP3(F12) t_{can}	MP3(F12) t_{PNO}
1	10^{-8}	5	15	15.2	17.6	140	38.5	455	51.4	120	0.05	5.6	5.5	0.05	9.9	8.8
2	10^{-8}	9	26	16.6	21.1	244	30.5	797	39.2	351	0.06	44.1	35.2	0.05	126.9	80.7
4	10^{-5}	17	48	11.8	16.4	452	5.1	1481	4.6	1135	2.21	550	231	1.89	2928	346
4	10^{-6}	”	”	13.4	18.0	”	8.8	”	8.7	”	0.67	”	262	0.54	”	465
4	10^{-7}	”	”	15.0	19.4	”	13.8	”	15.1	”	0.21	”	310	0.16	”	808
4	10^{-8}	”	”	16.9	21.3	”	23.1	”	28.2	”	0.07	”	323	0.05	”	871
4	10^{-9}	”	”	20.1	24.8	”	40.7	”	54.0	”	0.02	”	391			
8	10^{-8}	33	92	16.1	20.1	868	18.8	2849	22.2	3058	0.07	11519	3977			

Downloaded 24 May 2012 to 134.147.252.238. Redistribution subject to AIP license or copyright; see http://jcp.aip.org/about/rights_and_permissions

Compared to their conventional counterparts, the explicitly correlated PNO calculations need for a given truncation threshold T_{PNO} significantly less PNOs and, moreover, they exhibit a smaller truncation error. For example, for the tetrapeptide $(\mathrm{glycine})_4$ in the aug-cc-pVDZ basis OSV-PNO-MP2 uses for $T_{\mathrm{PNO}} = 10^{-8}$ on average 34.4 PNOs (almost 50% more than the F12 method) but has still a truncation error of 0.04%, twice as large as the F12 method. Therefore, the geminal contribution corrects for a large part of the contribution from the discarded PNOs. At the MP3 level, the smaller number of PNOs in the explicitly correlated variant also reduces the memory and disk space demands for the integrals $g^{\bar{c}\bar{d}}_{\bar{a}\bar{b}}$ which scale with the fourth power of the number of PNOs per pair.

In Table II we listed the average number of V-PNOs, O-PNOs, and CA-PNOs per pair. With increasing lengths of the glycine chain the average number of CA-PNOs $\bar{a}'_{ij}$ for the projector ${}^{B}\hat{Q}_{ij}$, which is used for the intermediate $\mathcal{U}^{ij}_{\bar{a}\bar{b}}$, decreases most rapidly. For the glycine monomer the ratio V-PNOs:CA-PNOs is about 1:1.34, but the octapeptide ratio has decreased to 1:1.18, despite the fact that the CA-PNOs are truncated with a slightly tighter threshold ($10^{-8.5}$) than the V-PNOs (10^{-8}). This reflects the more short-range character of the integrals $r^{ij}_{a'b}$ compared to the cluster amplitudes t^{ij}_{ab}. The average number of $\bar{\bar{K}}_{ij}$ and $\bar{K}_{ij}$ O-PNOs per pair used in the projector ${}^{A}\hat{Q}_{ij}$, however, decreases in this regime of system sizes and with a truncation threshold of $10^{-9.5}$ somewhat slower than the number of V-PNOs.

To elucidate the relative OSV and PNO truncation errors for the virtual and auxiliary orbitals, we have performed OSV-PNO-MP2-F12 and PNO-MP2-F12 calculations on the ethylenedioxy-tetrathiafulvalene (EDO-TTF) molecule in the aug-cc-pVDZ basis. EDO-TTF has the same number of atoms as the glycine dipeptide and has previously been used to benchmark the MP2-F12 method.[48] We used for these calculations the optimised CA basis from Ref. 58 with an exponent of 1.0 for the Slater-type correlation factor. In Table III we report the overall truncation error, compared to the canonical result for $T_{\mathrm{PNO}} = 10^{-6}$, 10^{-7}, and 10^{-8} and for $T_{\mathrm{OSV}} = T_{\mathrm{PNO}}$, $T_{\mathrm{OSV}} = 0.1\,T_{\mathrm{PNO}}$, and no OSV truncation (i.e., the PNO-MP2-F12 method). The default values of $T_{\mathrm{X\text{-}PNO}}$ were selected, where $T_{\mathrm{X\text{-}PNO}}$ are related to T_{PNO} in the manner prescribed in Ref. 49. For these tests we set $T_{\mathrm{OSX}} = T_{\mathrm{X\text{-}PNO}}$.

TABLE III. Truncation errors (in mH/atom) for the MP2-F12/aug-cc-pVDZ correlation energy of EDO-TTF for the PNO and hybrid OSV-PNO methods, with PNO thresholds between 10^{-6} and 10^{-8}. For OSV-PNO-MP2-F12 values, OSV truncation thresholds $T_{\mathrm{OSV}} = T_{\mathrm{PNO}}$ and $T_{\mathrm{OSV}} = 0.1\,T_{\mathrm{PNO}}$ are tabulated (for PNO-MP2-F12 there is no initial OSV truncation). $\%T_{\mathrm{OSV}}$ and $\%T_{\mathrm{PNO}}$ are, respectively, the percentages of double excitation amplitudes kept after the OSV and the PNO truncation of the virtual space. The basis set limit valence correlation energy is −2.758(2) and the basis set error for the canonical MP2-F12/aug-cc-pVDZ value is 3.15 mH/atom.

	$T_{\mathrm{OSV}} = T_{\mathrm{PNO}}$		$T_{\mathrm{OSV}} = 0.1\,T_{\mathrm{PNO}}$		PNO-MP2	
T_{PNO}	Δ_{trunc}	$\%T_{\mathrm{OSV}}$	Δ_{trunc}	$\%T_{\mathrm{OSV}}$	Δ_{trunc}	$\%T_{\mathrm{PNO}}$
10^{-6}	1.76	0.9	1.27	2.6	1.09	0.1
10^{-7}	0.61	2.9	0.44	6.9	0.39	0.4
10^{-8}	0.19	6.9	0.14	15.2	0.13	1.2

TABLE IV. Truncation errors (μH/atom) due to truncation of the X-PNO and X-OSV spaces in OSV-PNO-MP2-F12 calculations on EDO-TTF in an aug-cc-pVDZ basis. N_X is the number of X-OSVs (or X-PNOs for $T_{\mathrm{OSV}} = 0$) that survive truncation. EDO-TTF has 67 occupied orbitals and 1447 virtual orbitals (HF plus CABS).

		$\bar{\bar{K}}_{ij}$		$\bar{K}_{ij}$		$\bar{a}'_{ij}$	
T_{PNO}	T_{OSV}	Δ_{trunc}	N_X	Δ_{trunc}	N_X	Δ_{trunc}	N_X
10^{-6}	$T_{\mathrm{X\text{-}PNO}}$	−6.26	34	−4.23	46	30.2	130
	$0.1\,T_{\mathrm{X\text{-}PNO}}$	−3.93	46	−4.21	59	15.7	210
	0	−3.86	15	−4.21	21	9.8	10
10^{-7}	$T_{\mathrm{X\text{-}PNO}}$	−2.31	38	−1.93	52	7.6	210
	$0.1\,T_{\mathrm{X\text{-}PNO}}$	−1.69	52	−1.92	61	2.9	319
	0	−1.68	17	−1.92	23	1.7	20
10^{-8}	$T_{\mathrm{X\text{-}PNO}}$	−0.83	45	−0.61	57	1.4	318
	$0.1\,T_{\mathrm{X\text{-}PNO}}$	−0.73	56	−0.60	63	0.4	465
	0	−0.72	20	−0.60	27	0.3	43

From Table III we see that setting $T_{\mathrm{OSV}} = 0.1\,T_{\mathrm{PNO}}$ ensures that the additional truncation error due to the use of OSVs as pre-PNOs is less than 20% of the overall truncation error. Although this is slightly larger than we would like, it is acceptably small. The percentage of double excitation amplitudes kept after OSV and after PNO truncation, also reported in Table III, confirms that PNO truncation reduces the dimension of the OSV double excitation space by a factor of 5–15, just as for the OSV-PNO-MP2 calculations without the geminal basis (Table I).

In Table IV we report contributions to the overall truncation error arising from truncation of the OSX and X-PNO basis sets. These were computed as the difference between a calculation with all OSVs, OSXs, V-PNOs, and X-PNOs truncated and a similar calculation where only the orbital space under investigation was not truncated. The values of $T_{\mathrm{X\text{-}PNO}}$ are related to that of T_{PNO} in the standard way and for the evaluation of the CA truncation errors, the hybrid approximation was employed.[47,60] We see that for the O-PNOs, $T_{\mathrm{OSX}} = 0.1\,T_{\mathrm{X\text{-}PNO}}$ is more than sufficient to ensure that the OSX truncation error is an order of magnitude smaller than the X-PNO truncation error, which itself is more than an order of magnitude smaller than the V-PNO truncation error. For the CA-PNOs of the ${}^{B}\hat{Q}_{12}$ projector, this choice leads to approximately equal OSX and CA-PNO truncation errors. Since this combined error is still an order of magnitude smaller than the V-PNO truncation error and since the costs are sensitive to the dimension of the orbital-specific complementary auxiliary (OS-CA) basis, we are satisfied with the choice $T_{\mathrm{OSX}} = 0.1\,T_{\mathrm{X\text{-}PNO}}$ for all auxiliary orbitals.

C. Performance of PNO-MP2.5(F12) for intermolecular interactions

A typical application of Møller-Plesset perturbation theory is the computation of the interaction energies of weakly bound complexes. Pitoňák *et al.*[61] found recently that the half and half interpolation between MP2 and MP3, denoted

Downloaded 24 May 2012 to 134.147.252.238. Redistribution subject to AIP license or copyright; see http://jcp.aip.org/about/rights_and_permissions

MP2.5,

$$E_{\mathrm{MP2.5}} = E_{\mathrm{MP2}} + \tfrac{1}{2} E_{\mathrm{MP3}} \tag{65}$$

is for weak intermolecular interactions in many cases a very close approximation to CCSD(T). For the S66 data set[62] it has a root mean square error (RMSD) with respect to the CCSD(T) reference below 0.2 kcal/mol. In particular, MP2.5 gives a well-balanced description of hydrogen-bonded and π-stacked interactions. Weak intermolecular interactions are on the other hand very sensitive to imbalances in the electronic structure calculations for the complex and the isolated monomers and are thus a stringent test for approximate methods, such as PNO theory. The S22 set[63] was recently also employed by Liakos *et al.*[64] to test the LPNO-CEPA/1 method for intermolecular interactions. They could show that LPNO-CEPA/1 with modest PNO truncation thresholds achieves an RMSD of 0.24 kcal/mol if combined with an MP2 complete basis set estimate.

The question we want to address is how the PNO truncation errors for the intermolecular binding energies compare to the total deviation from the basis set limit, to identify recommendable combinations with a good accuracy/cost ratio. To get highly accurate reference values with known very small basis set errors we employed the MP3(F12) method implemented in the TURBOMOLE package and computed, for the 12 smallest complexes (structures 1–3, 5, 6, 8–10, 12, 51, 59, and 60) of the S66 data set,[62] interaction energies close to the basis set limit using the aug-cc-pwCV5Z[65] basis for C, N, O, and the aug-cc-pV5Z[56] for H. As CA basis we used the aug-cc-pwCV5Z (C, N, O) and aug-cc-pV5Z (H) density-fitting basis sets from Ref. 59 and for density-fitting in the Fock matrix evaluation the aug-cc-pV5Z basis from Ref. 66. For the density-fitting of all remaining integrals used in the MP2-F12 and MP3(F12) correlation treatments we used the MP2-optimised aug-cc-pV6Z density-fitting basis[59] which has been augmented by a set of steep 4s3p5d2f1g functions for C, N, O, and 4s3p4d2f1g for H. The $1s^2$ core of the non-hydrogen atoms has been frozen in all correlated calculations and an exponent of 1.4 was used for the Slater-type geminals. The counterpoise correction, which might be used as diagnostic for the remaining basis set errors was in these calculations for all 12 dimers below 0.0025 kcal/mol for interaction energies between −1.64 and −7.6 kcal/mol.

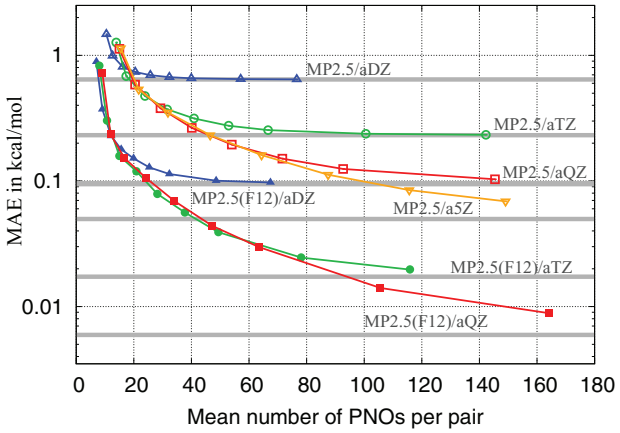


FIG. 4. Remaining PNO truncation and basis set errors in kcal/mol for PNO-MP2.5 and PNO-MP2.5(F12) calculations with the aug-cc-pVnZ basis sets with n = D (△), T (○), Q (□), and 5 (▽). (Filled symbols used for the F12 results.) The PNO calculations have been carried out for $-\log_{10} T_{\mathrm{PNO}} = 5$, 5.5, 6, 6.5, 7, 7.5, 8, 9, and 10. For MP2.5 calculations with the aug-cc-pVQZ basis the last point ($T_{\mathrm{PNO}} = 10^{-10}$) has been skipped and with the aug-cc-pV5Z basis the last two points were obtained with $T_{\mathrm{PNO}} = 10^{-8.5}$. Grey horizontal lines indicate the results for the full canonical MP2.5 and MP2.5(F12) calculations.

Fig. 4 summarises the results of the PNO-MP2.5 and PNO-MP2.5(F12) calculations for the 12 smallest weakly bound complexes of the S66 test set with the correlation-consistent aug-cc-pVnZ basis sets. We find that, just as in our previous work on PNO-MP2-F12 total and reaction energies, curves obtained with different cardinal numbers are for loose PNO thresholds almost on top of each other. The curves deviate at the point where the smaller basis set is exhausted and the respective curve flattens out, tending to the untruncated limit of this basis. Beyond these points, tighter PNO thresholds do not give significant improvements in the accuracy, but solely increase the costs. Without the geminal basis functions, the cross-over point for the aug-cc-pVDZ basis and aug-cc-pVTZ basis sets are, respectively, at $T_{\mathrm{PNO}} \approx 10^{-7}$ or ≈26 PNOs/pair, and $T_{\mathrm{PNO}} \approx 10^{-8}$ or ≈67 PNOs/pair. For the aug-cc-pVQZ basis the accuracy increases significantly up to $T_{\mathrm{PNO}} \approx 10^{-9}$. Again, using tighter thresholds will solely increase the computational costs but not give significantly higher accuracy. To elucidate the relation between computational costs, T_{PNO}, and basis set quality, we list in Table V for the methylamine (CH_3NH_2) dimer the wall clock time

TABLE V. PNO-MP3 and PNO-MP3(F12) calculations on the CH_3NH_2 dimer. Dependence of the wall clock time (t_{wall} in min) and accuracy on the PNO threshold, T_{PNO}, and the one-electron basis set. $\%_{corr}$ is the percentage of the correlation contribution to the counterpoise-corrected binding energy obtained, where 100% refers to estimated basis set limit.

	PNO-MP3								PNO-MP3(F12)					
	aug-cc-pVDZ		aug-cc-pVTZ		aug-cc-pVQZ		aug-cc-pV5Z		aug-cc-pVDZ		aug-cc-pVTZ		aug-cc-pVQZ	
$-\log T_{\mathrm{PNO}}$	t_{wall}	$\%_{corr}$	t_{wall}	$\%_{corr}$	t_{wall}	$\%_{corr}$	t_{wall}	$\%_{corr}$	t_{wall}	$\%_{corr}$	t_{wall}	$\%_{corr}$	t_{wall}	$\%_{corr}$
5	0.8	48.8	5.6	59.4	52	61.8	174	60.9	14	77.1	56	74.6	266	78.6
6	1.0	73.5	6.5	85.7	90	88.5	184	88.9	16	92.9	63	94.9	320	95.5
7	1.3	77.2	9.5	91.0	188	94.5	400	95.4	17	94.4	72	97.1	368	97.6
8	2.6	78.7	15.7	93.1	313	96.9	750	97.9	19	95.9	84	98.7	465	99.2
9	4.8	79.1	42.5	93.7	418	97.6			23	96.3	115	99.3	701	99.7
10	9.4	79.3	135.	93.9					31	96.5	204	99.5	877	99.9

Downloaded 24 May 2012 to 134.147.252.238. Redistribution subject to AIP license or copyright; see http://jcp.aip.org/about/rights_and_permissions

TABLE VI. MP2.5(F12)/aug-cc-pVTZ binding energies (in kcal/mol) for the uracil dimer in a π-stacked geometry. The truncation threshold for the PNO-MP3(F12) calculation was set to 10^{-8}.

	$\Delta E_{\text{CP-corr.}}$	t_{wall} (*h*)	Cores	PNO	OPNO-1	OPNO-2	CAPNO-B
Canonical	−9.4	48.6	12	862	58	58	1480
PNO, 10^{-8}	−9.3	80.9	1	37	16	15	47

and the percentage of the correlation contribution to the binding energy for the aug-cc-pV*n*Z basis sets and PNO thresholds between 10^{-5} and 10^{-10}. These results also show that it is not worth using large basis sets with loose thresholds, since the larger number of AOs greatly increases the computational costs for the integral evaluation, which even with the density-fitting approximation scale as $\mathcal{O}(\mathcal{M}^3)$ with the size of the atomic basis sets $\mathcal{M}$. The present results suggest that, for weak intermolecular interactions, it is not meaningful to use PNO truncation thresholds $>10^{-6}$ for aug-cc-pVTZ or $>10^{-7}$ for aug-cc-pVQZ. The aug-cc-pV5Z basis surpasses the aug-cc-pVQZ basis in accuracy only for $T_{\text{PNO}} \leq 10^{-8.5}$.

The explicitly correlated variants start to outperform the non-F12 methods for weak intermolecular interactions for target accuracies $\gtrapprox$94%, which is with PNO-MP2.5(F12) already reached in the aug-cc-pVDZ basis with $T_{\text{PNO}} = 10^{-7}$. With $T_{\text{PNO}} = 10^{-8}$ (on average only ≈35 PNOs per pair) the PNO-MP2.5(F12)/aug-cc-pVDZ results are about as accurate as PNO-MP2.5/aug-cc-pVQZ calculations with tight thresholds, which are an order of magnitude more costly. The results in the aug-cc-pVTZ basis, with the same threshold and on average 50 PNOs per pair, surpass the accuracy of the conventional aug-cc-pV5Z calculations. With $T_{\text{PNO}} = 10^{-10}$ and on average 115 and 164 PNOs per pair, the PNO-MP2.5(F12) calculations in aug-cc-pVTZ and aug-cc-pVQZ reach an accuracy that cannot be obtained by non-F12 calculations with standard basis sets. The results in Table V also show that using the aug-cc-pVTZ basis in the explicitly correlated calculations is only worthwhile with $T_{\text{PNO}} \leq 10^{-7}$ and that for aug-cc-pVQZ the threshold should not be higher than 10^{-9}.

As an example for the performance of the present, still preliminary, implementation of PNO-MP3(F12) for weak intermolecular complexes Table VI lists the results for the uracil $C_4H_4N_2O_2$ dimer in the π-stacked structure from the S66 test set in the aug-cc-pVTZ basis (920 basis and 1480 CABS functions). The canonical calculation, run on 12 CPU cores, took almost 49 h. With the PNO implementation and $T_{\text{PNO}} = 10^{-8}$ the calculation could be completed in 80.9 h, on a single core. The error in the binding energy due to the PNO truncation is ≈0.1 kcal/mol or 1%. Based on the benchmark results for the 12 smallest dimers from the S66 test set we expect the remaining basis set error to be of the same order of magnitude.

VIII. SUMMARY AND CONCLUSIONS

The recently conceived OSV and the revived PNO approaches share the common goal of exploiting localisation to arrive at low scaling computational electronic structure methods without invoking *a priori* assumptions of the extent of locality in a molecule, such that the error with respect to an analogous canonical calculation can be controlled through a single, user specified parameter. Both of these localisation approaches combine well with F12 explicitly correlated methods, which dramatically reduce the number of necessary AO basis functions per atom required for a given basis set incompleteness error. In both approaches the local truncated basis sets are determined by analysing an approximate wavefunction so that they automatically adapt to the physics of the target wavefunction, which is an important feature for response methods where often state- or perturbation-specific non-local polarisation and charge-transfer effects need to be described.[35]

The OSV and PNO representations of the doubles amplitudes in pair theories have complementary characteristics. In OSV methods, the correlating orbitals are specific to each occupied orbital, whereas in PNO methods they are specific to each occupied pair. In OSV methods, therefore, the cost of building the OSV vectors and transforming integrals into this basis is much smaller than the corresponding costs in PNO methods. Conversely, the space of doubles amplitudes required for a given target accuracy in PNO methods is an order of magnitude smaller than in OSV methods, and the cost of the contractions of amplitudes and integrals is therefore substantially reduced.

We have presented a hybrid OSV-PNO approach for computing MP2 and MP3 energies and their explicitly correlated counterparts MP2-F12 and MP3(F12), that combines the advantages of the two representations. First, OSVs and pair energy estimates are constructed at a cost that scales as $\mathcal{O}(\mathcal{N}^4)$ with system size $\mathcal{N}$. Subsequently PNOs for pair *ij* are constructed from the basis of unified OSVs for *i* and *j*. For the F12 variants, we ensure that contractions over the auxiliary orbitals in the F12 RI approximation are low scaling by defining OSXs and X-PNOs for these auxiliary orbital spaces in an analogous manner to the OSVs and PNOs for the virtual orbitals.

The relationship between the X-PNO and PNO truncation thresholds that ensures that errors in the F12 RI are an order of magnitude smaller than the basis set truncation error have been established previously.[49] We find that setting the occupation number threshold for the OSV and OSX vectors one order of magnitude smaller than the PNO and X-PNO truncation thresholds, respectively, ensures that the overall truncation error is determined solely by the PNO threshold and that the energy converges smoothly to the canonical result as this threshold is reduced.

With the hybrid OSV-PNO approach MP2 and MP3 can be implemented with a computational cost that scales at most with $\mathcal{O}(\mathcal{N}^4)$ and outperform the canonical implementations of RI-MP2 and MP3 even with conservatively tight truncation thresholds. For the $(\text{glycine})_{16}$ polypeptide an OSV-PNO-MP2 calculation with a threshold of 10^{-8} in the aug-cc-pVTZ basis with 4140 basis functions takes 37 CPU hours (on Intel Xeon E5430 2.66 GHz) and is still much faster than the underlying HF-SCF calculation. The PNO truncation error is only <0.5%, i.e., more than an order of magnitude smaller than the basis set incompleteness error for the aug-cc-pVTZ basis.

Downloaded 24 May 2012 to 134.147.252.238. Redistribution subject to AIP license or copyright; see http://jcp.aip.org/about/rights_and_permissions

The combination with the explicitly correlated F12 methods not only dramatically enhances the convergence with the one-electron basis set but also the convergence to the untruncated limit with increasing number of PNOs. Altogether, this greatly reduces the number of PNOs and the computational costs for achieving a given target accuracy. For weak intermolecular interactions the PNO-F12 methods recover with the aug-cc-pVDZ basis and a truncation threshold of 10^{-8} more 95% of the basis set limit correlation contribution to the binding energy. With non-F12 methods the costs for achieving this accuracy are about an order of magnitude higher.

Interestingly, Krause and Werner have very recently[50] used a simulated approach to compare the PAO, OSV, and PNO methods for CCSD and CCSD-F12x,[67] and have also reached the conclusion that a hybrid OSV-PNO scheme is an excellent way forward.

Our present implementation is still preliminary. It only partially makes use of local density-fitting and uses OSVs currently only for the construction of the PNOs, not yet to reduce the computational effort for building the integrals for the U, V, W intermediates. Even so, we see early break-even points with the canonical implementations in the TURBOMOLE package.[45,48,53] For MP3 and its F12 variant the generation of the integrals for the intermediates U and V (and for F12 in addition $\mathcal{U}$ and $\mathcal{V}$) are the time-determining step. For both we expect that the costs can be considerably reduced by computing the PNO integrals from intermediates in the OSV basis. This could also reduce the storage and I/O demands for the integrals, which is another severe bottleneck of the PNO methods beyond MP2 if a high accuracy is desired. This bottleneck is particularly severe for non-F12 methods which require a larger number of PNOs.

Based on the results for weak intermolecular interactions presented in Sec. VII C, we make the following recommendations regarding basis sets and truncation thresholds:

- aug-cc-pVDZ without F12 and $T_{\mathrm{PNO}} = 10^{-7}$ for qualitative calculations recovering ≈77% of the correlation contribution;
- aug-cc-pVTZ without F12 and $T_{\mathrm{PNO}} = 10^{-7}$ for a semi-quantitative accuracy of ≈90% for the correlation contribution;
- aug-cc-pVDZ with F12 and $T_{\mathrm{PNO}} = 10^{-8}$ for an accuracy of ≈95%;
- aug-cc-pVTZ with F12 and $T_{\mathrm{PNO}} = 10^{-7}$–$10^{-10}$ for good quantitative and up to benchmark accuracies of 97% –99.5% of the basis set limit.

Using the non-F12 methods with tighter truncation thresholds or basis sets larger than aug-cc-pVTZ or the F12 methods with looser thresholds reduces the accuracy:cost ratios. With the F12 methods the aug-cc-pVQZ basis is only needed for very high accuracies.

PNO–MP3(F12) calculations with $T_{\mathrm{PNO}} = 10^{-8}$ can already with the present implementation be performed on systems with 20–30 atoms within a few days CPU time. F12 explicitly correlated PNO methods thus open a route for accurate calculations on larger intermolecular complexes than possible with canonical implementations. Future extensions to PNO-CEPA(F12*) or PNO-CCSD(F12*), currently in progress in our laboratories, will further expand the applicability of the approach to reactions energies and other properties for larger systems. The combination of PNOs with OSVs and the possibility to transform between the two representations introduce a flexibility for the implementation of PNO methods which can diminish some bottlenecks of the current implementations. OSVs are also a natural choice for representing single excitations and might also facilitate an efficient implementation of triple excitations in a PNO-like framework.

ACKNOWLEDGMENTS

D.P.T. thanks the Royal Society for support from the University Research Fellow scheme and B.H. thanks the TURBOMOLE GmbH for financial support.

[1] T. Helgaker, W. Klopper, and D. P. Tew, Mol. Phys. **106**, 2107 (2008).
[2] S. F. Boys, in *Quantum Theory of Atoms, Molecules and the Solid State*, edited by P. O. Löwdin (Academic, New York, 1966), p. 253.
[3] J. Pipek and P. G. Mezey, J. Chem. Phys. **90**, 4916 (1989).
[4] B. Jansík, S. Høst, K. Kristensen, and P. Jørgensen, J. Chem. Phys. **134**, 194104 (2011).
[5] P. Pulay, Chem. Phys. Lett. **100**, 151 (1983).
[6] S. Saebo and P. Pulay, Chem. Phys. Lett. **113**, 13 (1985).
[7] S. Saebo and P. Pulay, Ann. Rev. Phys. Chem. **44**, 213 (1993).
[8] M. Schütz, Phys. Chem. Chem. Phys. **4**, 3941 (2002).
[9] H.-J. Werner, F. R. Manby, and P. J. Knowles, J. Chem. Phys. **118**, 8149 (2003).
[10] H.-J. Werner and M. Schütz, J. Chem. Phys. **135**, 144116 (2011).
[11] F. R. Manby, H.-J. Werner, T. B. Adler, and A. J. May, J. Chem. Phys. **124**, 094103 (2006).
[12] H.-J. Werner, J. Chem. Phys. **129**, 101103 (2008).
[13] T. B. Adler and H.-J. Werner, J. Chem. Phys. **130**, 241101 (2009).
[14] T. B. Adler and H.-J. Werner, J. Chem. Phys. **135**, 144117 (2011).
[15] W. Kutzelnigg, Theor. Chem. Acc. **68**, 445 (1985).
[16] W. Klopper, F. R. Manby, S. Ten-no, and E. F. Valeev, Int. Rev. Phys. Chem. **25**, 427 (2006).
[17] C. Hättig, W. Klopper, A. Köhn, and D. P. Tew, Chem. Rev. **112**, 4 (2012).
[18] L. Kong, F. A. Bischoff, and E. F. Valeev, Chem. Rev. **112**, 75 (2012).
[19] H.-J. Werner, T. B. Adler, G. Knizia, and F. R. Manby, in *Recent Progress in Coupled Cluster Methods: Theory and Applications*, edited by P. Cársky, J. Pittner, and J. Paldus (Springer, 2009), pp. 1–47.
[20] N. Flocke and R. J. Bartlett, J. Chem. Phys. **121**, 10935 (2004).
[21] T. F. Hughes, N. Flocke, and R. J. Bartlett, J. Phys. Chem. A **112**, 5994 (2008).
[22] M. Ziółkowski, B. Jansík, T. Kjærgaard, and P. Jørgensen, J. Chem. Phys. **133**, 014107 (2010).
[23] K. Kristensen, M. Ziółkowski, B. Jansík, T. Kjærgaard, and P. Jørgensen, J. Chem. Theory Comput. **7**, 1677 (2011).
[24] H. Stoll, Phys. Rev. B **46**, 6700 (1992).
[25] H. Stoll, Chem. Phys. Lett. **191**, 548 (1992).
[26] J. Friedrich and M. Dolg, J. Chem. Theory Comput. **5**, 287 (2009).
[27] J. Friedrich, D. P. Tew, W. Klopper, and M. Dolg, J. Chem. Phys. **132**, 164114 (2010).
[28] K. Walczak, J. Friedrich, and M. Dolg, Chem. Phys. **376**, 36 (2010).
[29] W. Li, P. Piecuch, J. R. Gour, and S. Li, J. Chem. Phys. **131**, 114109 (2009).
[30] F. Neese, F. Wennmohs, and A. Hansen, J. Chem. Phys. **130**, 114108 (2009).
[31] F. Neese, A. Hansen, and D. G. Liakos, J. Chem. Phys. **131**, 064103 (2009).
[32] L. M. J. Huntington, A. Hansen, F. Neese, and M. Nooijen, J. Chem. Phys. **136**, 064101 (2012).
[33] W. Meyer, Int. J. Quantum Chem. Symp. **5**, 341 (1971).
[34] D. P. Tew, B. Helmich, and C. Hättig, J. Chem. Phys. **135**, 074107 (2011).
[35] B. Helmich and C. Hättig, J. Chem. Phys. **135**, 214106 (2011).
[36] J. Yang, Y. Kurashige, F. R. Manby, and G. K.L. Chan, J. Chem. Phys. **134**, 044123 (2011).
[37] Y. Kurashige, J. Yang, G. K.-L. Chan, and F. R. Manby, J. Chem. Phys. **136**, 124106 (2012).

Downloaded 24 May 2012 to 134.147.252.238. Redistribution subject to AIP license or copyright; see http://jcp.aip.org/about/rights_and_permissions

[38]S. Ten-no, Chem. Phys. Lett. **398**, 56 (2004).
[39]D. P. Tew and W. Klopper, J. Chem. Phys. **123**, 074101 (2005).
[40]S. Ten-no, J. Chem. Phys. **121**, 117 (2004).
[41]D. P. Tew and W. Klopper, Mol. Phys. **108**, 315 (2010).
[42]E. F. Valeev, Chem. Phys. Lett. **395**, 190 (2004).
[43]H. Fliegl, W. Klopper, and C. Hättig, J. Chem. Phys. **122**, 084107 (2005).
[44]A. Köhn and D. P. Tew, J. Chem. Phys. **133**, 174117 (2010).
[45]C. Hättig, D. P. Tew, and A. Köhn, J. Chem. Phys. **132**, 231102 (2010).
[46]W. Klopper and C. C. M. Samson, J. Chem. Phys. **116**, 6397 (2002).
[47]H.-J. Werner, T. B. Adler, and F. Manby, J. Chem. Phys. **126**, 164102 (2007).
[48]R. A. Bachorz, F. A. Bischoff, A. Glöß, C. Hättig, S. Höfener, W. Klopper, and D. P. Tew, J. Comput. Chem. **32**, 2492 (2011).
[49]D. P. Tew and C. Hättig, "Pair natural orbitals in explicitly-correlated second order Moller-Plesset theory," Int. J. Quantum Chem. (to be published).
[50]C. Krause and H.-J. Werner, "Comparison of explicitly correlated local coupled-cluster methods with various choices of virtual orbitals," Phys. Chem. Chem. Phys. (to be published).
[51]TURBOMOLE development version (2012), for further information see http://www.turbomole.com.
[52]M. Häser and R. Ahlrichs, J. Comp. Chem. **10**, 104 (1989).
[53]C. Hättig and F. Weigend, J. Chem. Phys. **113**, 5154 (2000).
[54]TURBOMOLE, version 6.3 2011, a development of University of Karlsruhe and Forschungszentrum Karlsruhe GmbH, 1989–2007, TURBOMOLE GmbH, 2007, see http://www.turbomole.com.
[55]F. Weigend, A. Köhn, and C. Hättig, J. Chem. Phys. **116**, 3175 (2001).
[56]T. H. Dunning, J. Chem. Phys. **90**, 1007 (1989).
[57]R. A. Kendall, T. H. Dunning, and R. J. Harrison, J. Chem. Phys. **96**, 6796 (1992).
[58]K. Yousaf and K. Peterson, Chem. Phys. Lett. **476**, 303 (2009).
[59]C. Hättig, Phys. Chem. Chem. Phys. **7**, 59 (2005).
[60]W. Klopper, J. Chem. Phys. **120**, 10890 (2004).
[61]M. Pitoňák, P. Neogrády, J. Černý, S. Grimme, and P. Hobza, ChemPhysChem **10**, 282 (2009).
[62]J. Řezáč, K. E. Riley, and P. Hobza, J. Chem. Theory Comput. **7**, 2427 (2011).
[63]P. Jurečka, J. Šponer, J. Černý, and P. Hobza, Phys. Chem. Chem. Phys. **8**, 1985 (2006).
[64]D. G. Liakos, A. Hansen, and F. Neese, J. Chem. Theory Comput. **7**, 76 (2011).
[65]K. A. Peterson and T. H. Dunning, J. Chem. Phys. **117**, 10548 (2002).
[66]F. Weigend, J. Comput. Chem. **29**, 167 (2007).
[67]G. Knizia, T. B. Adler, and H.-J. Werner, J. Chem. Phys. **130**, 054104 (2009).

Downloaded 24 May 2012 to 134.147.252.238. Redistribution subject to AIP license or copyright; see http://jcp.aip.org/about/rights_and_permissions